

## Unimolecular Decay Dynamics of Electronically Excited $\text{HCO}(A^1\Delta^1)$ : Rotational Control of Nonadiabatic Transitions

Ge Sun,<sup>a,#</sup> Shanyu Han,<sup>b,#</sup> Xianfeng Zheng,<sup>a,c</sup> Yu Song,<sup>a</sup> Yuan Qin,<sup>a</sup> Richard Dawes,<sup>d</sup> Daiqian Xie,<sup>e</sup> Hua Guo,<sup>b,\*</sup> and Jingsong Zhang<sup>a,\*</sup>

<sup>a</sup>*Department of Chemistry, University of California Riverside, Riverside, CA 92521, USA*

<sup>b</sup>*Department of Chemistry and Chemical Biology, University of New Mexico, Albuquerque, NM 87131, USA*

<sup>c</sup>*Anhui Province Key Laboratory of Optoelectric Materials Science and Technology, Department of Physics, Anhui Normal University, Wuhu, Anhui 241000, China*

<sup>d</sup>*Department of Chemistry, Missouri University of Science and Technology, Rolla, MO 65409, USA*

<sup>e</sup>*Institute of Theoretical and Computational Chemistry, Key Laboratory of Mesoscopic Chemistry, School of Chemistry and Chemical Engineering, Nanjing University, Nanjing 210093, China*

### Supporting Information

#: these two authors contributed equally.

\*: corresponding authors, emails: [jszhang@ucr.edu](mailto:jszhang@ucr.edu), [hguo@unm.edu](mailto:hguo@unm.edu)

## S1. Experimental

The CO product internal energy distributions were converted from the H + CO product CM translational distributions. The CO product internal energy distributions were then deconvoluted by fitting with peaks of the CO rotational states in the  $\nu=0$  and  $\nu=1$  levels (the peak positions were established with the well-known molecular spectroscopic parameters of CO). The spacing of the peaks observed in the measured product energy distributions were close to those of the CO rotational states in the  $\nu=0$  vibrational level, indicating that CO ( $\nu=0$ ) was the main product from the photodissociation of HCO ( $\overset{\circ}{A}''$ ). In the deconvolution process, the peaks that correlate to the rotational states of  $\nu=0$  vibrational level, ( $\nu=0, j$ ) states, were put in the simulated CO product internal energy distributions first, then the gaps were filled with the peaks from the ( $\nu=1, j$ ) states. The fitting was then adjusted by varying the height of all the peaks to best match the calculated CO internal energy distributions to the experimental ones. For the photodissociation of the HCO ( $\overset{\circ}{A}''$ ) ( $1, 9^0, 0$ ) state, the best estimated CO vibrational population ratio was  $P(\nu=0):P(\nu=1) = 0.84 : 0.16$ , in excellent agreement with the theoretical result of  $P(\nu=0):P(\nu=1) = 0.84 : 0.16$ . Note that due to the overlap of a number of CO rotational states from  $\nu=0$  and  $\nu=1$  in the CO internal energy distribution, there was some uncertainty in the fitting. The vibrational population ratio of  $P(\nu=0):P(\nu=1) = 0.67 : 0.33$  gave an upper bound for the  $\nu=1$  contribution. The deconvolution processes of the HCO( $\overset{\circ}{A}''$ ) ( $1, 8^1, 0$ ) and ( $1, 10^1, 0$ ) were similar. The best estimated CO vibrational population ratio  $P(\nu=0):P(\nu=1)$  were  $0.87 : 0.13$  for ( $1, 8^1, 0$ ) and  $0.81 : 0.19$  for ( $1, 10^1, 0$ ), respectively. The range of the relative populations between the  $\nu=0$  and  $\nu=1$  products were summarized in Table S-I for the three vibronic resonances investigated in this work. As the contributions of the CO  $\nu=1$  product were small, varying the contributions of CO  $\nu=1$  product would not change the bimodal rotational distributions of the CO  $\nu=0$  product.

## S2. Theoretical

The Boltzmann factors for low-lying rotational states of HCO( $\overset{0}{X}^1A'$ ) are provided in Table S-II.

The CO( $v=0$ ) rotational distribution in the single transition ( $J=1 \leftarrow J_i=0$ ) for the (1, 8<sup>1</sup>, 0) resonance is shown in Figure S8 in comparison with the earlier theoretical result of Goldfield and coworkers.<sup>1</sup> While both show double peak at high  $j$  states, there are quantitative differences due presumably to the different potentials and the reduced dimensional model used in the earlier work.

1. E. M. Goldfield, S. K. Gray and L. B. Harding, *J. Chem. Phys.*, 1993, **99**, 5812-5827.
2. D. W. Neyer, S. H. Kable, J. C. Loison, P. L. Houston, I. Burak and E. M. Goldfield, *J. Chem. Phys.*, 1992, **97**, 9036-9045.
3. S. Han, X. Zheng, S. Ndengué, Y. Song, R. Dawes, D. Xie, J. Zhang and H. Guo, *Science Advances*, 2019, **5**, eaau0582.

**Table S-I.** Experimental CO product vibrational distribution ( $v=0$  and  $v=1$ ) from photodissociation of HCO via different vibrational levels in the  $\tilde{A}^2A''$  state. The range of the populations from fitting of the CM product translational energy distribution are listed.

level	$P(v=0)$	$P(v=1)$
(1, 8 <sup>1</sup> , 0)	0.72-0.87	0.28-0.13
(1, 9 <sup>0</sup> , 0)	0.67-0.84	0.33-0.16
(1, 10 <sup>1</sup> , 0)	0.71-0.81	0.29-0.19

**Table S-II.** Energies and Boltzmann factors ( $(2J_i + 1)e^{-E_{J_i}/kT}$ ) of the lowest-lying rotational states of HCO( $\tilde{X}^2A'$ ) at the experimental temperature (20K). The states are listed in ascending order of energy.

Rotational State	Energy (cm <sup>-1</sup> )	Boltzmann Factor
0 <sub>00</sub>	2801.20	1
1 <sub>01</sub>	2804.09	2.44
2 <sub>02</sub>	2809.87	2.68
3 <sub>03</sub>	2818.55	2.01
1 <sub>11</sub>	2827.07	0.47
1 <sub>10</sub>	2827.16	0.46
4 <sub>04</sub>	2830.11	1.12
2 <sub>12</sub>	2832.76	0.52
2 <sub>11</sub>	2833.04	0.51
3 <sub>13</sub>	2841.29	0.39
3 <sub>12</sub>	2841.86	0.38
5 <sub>05</sub>	2844.57	0.49
4 <sub>14</sub>	2852.68	0.22
4 <sub>13</sub>	2853.62	0.21
5 <sub>15</sub>	2866.89	0.098
5 <sub>14</sub>	2868.31	0.088
2 <sub>20</sub>	2901.60	0.0038
2 <sub>21</sub>	2901.60	0.0038
3 <sub>21</sub>	2910.28	0.0027
3 <sub>22</sub>	2910.27	0.0027

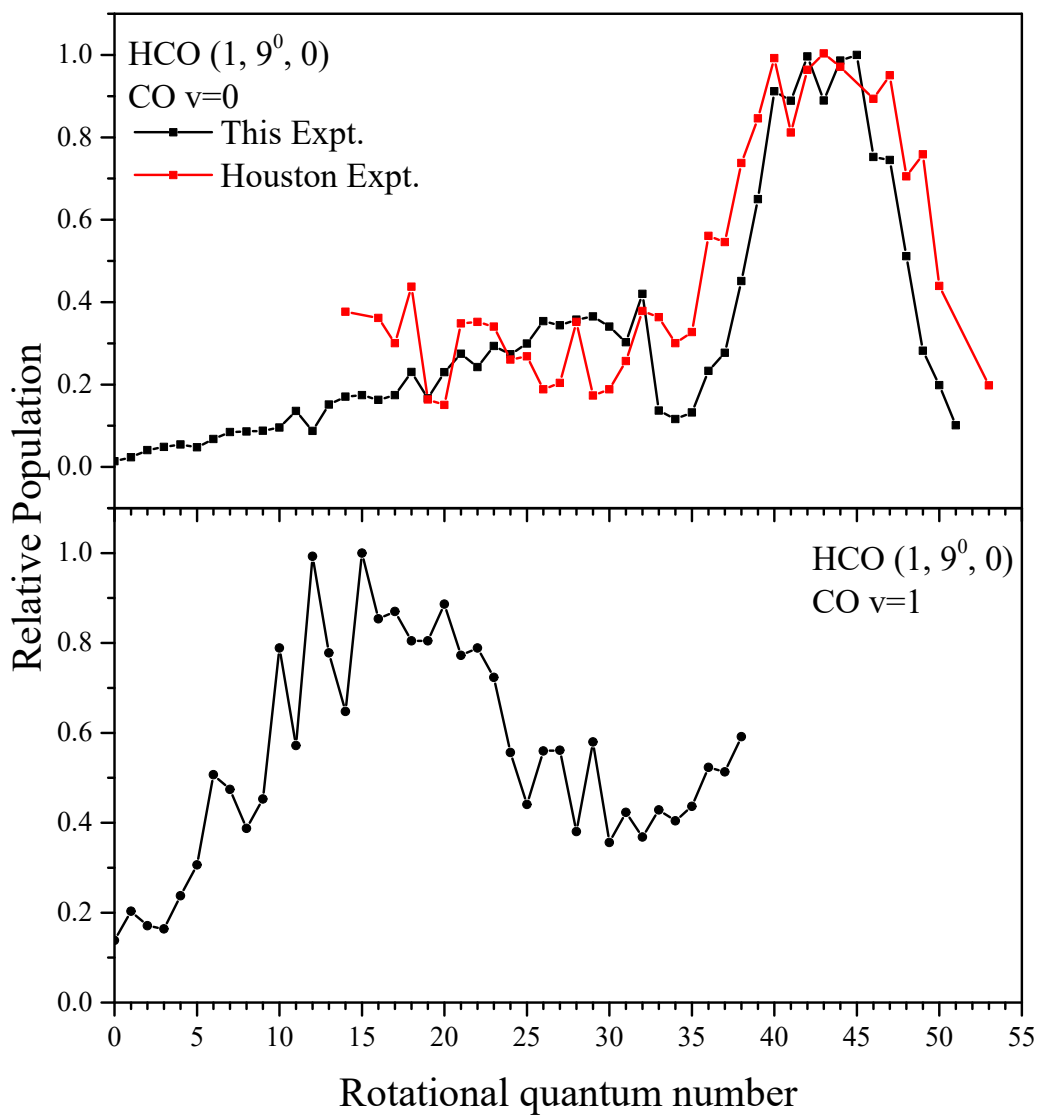


Figure S1. CO ( $X^1\Sigma^+$ ,  $v=0$  and 1) product rotational state distributions from the photodissociation of the HCO  $\tilde{A}^2A''(1, 9^0, 0)$  state. The black dots are the data from this experiment, and the red dots are data from Houston and coworkers.<sup>2</sup>

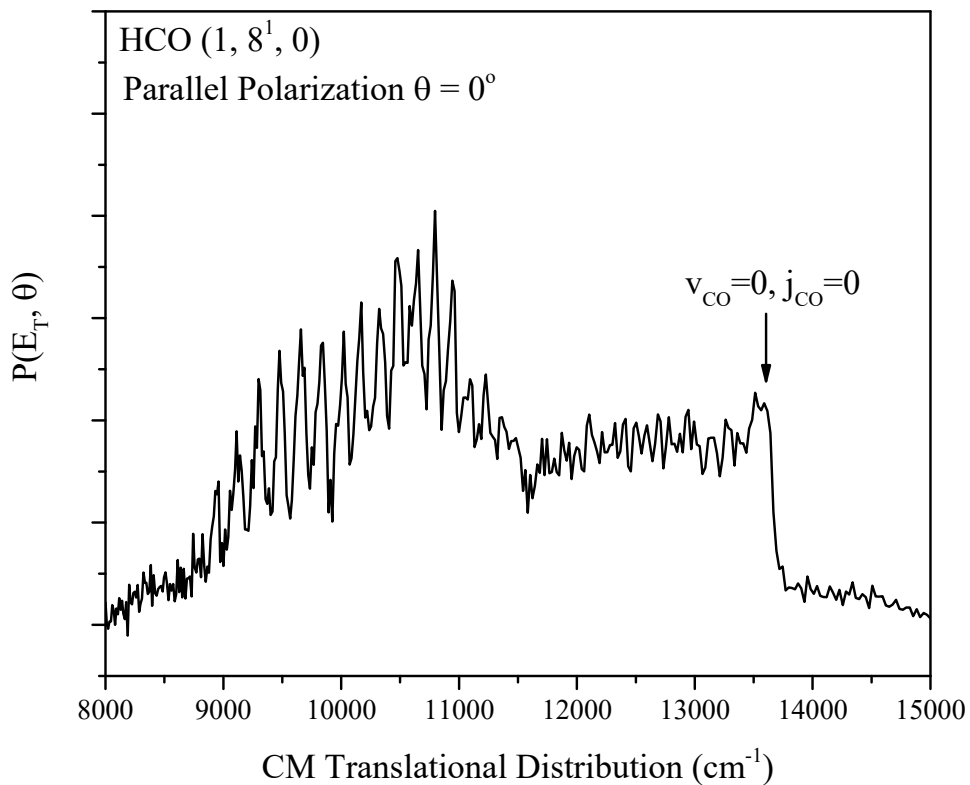


Figure S2. H + CO product CM translational energy distribution from the photodissociation of the HCO  $\tilde{A}^2A''(1, 8^1, 0)$  state. The product translational energy of the rovibrational ground state ( $\nu=0$ ,  $j=0$ ) CO product is indicated by an arrow.

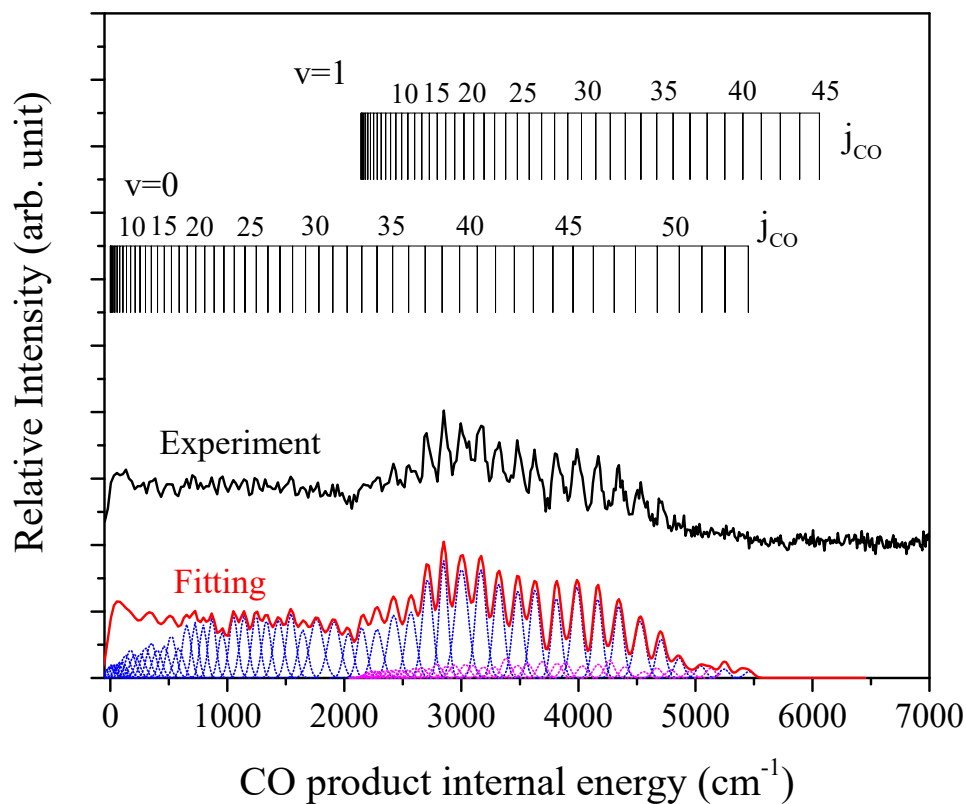


Figure S3. CO ( $X^1\Sigma^+$ ,  $v=0$  and 1) product internal energy distribution and the fitting result for the photodissociation of the HCO ( $\tilde{A}^2A''$ ) ( $1, 8^1, 0$ ) state. The blue and purple dot lines are the Gaussian peaks for each CO product rovibrational state for  $v=0$  and  $v=1$  levels, respectively. The red solid line is the sum of the Gaussian peaks.

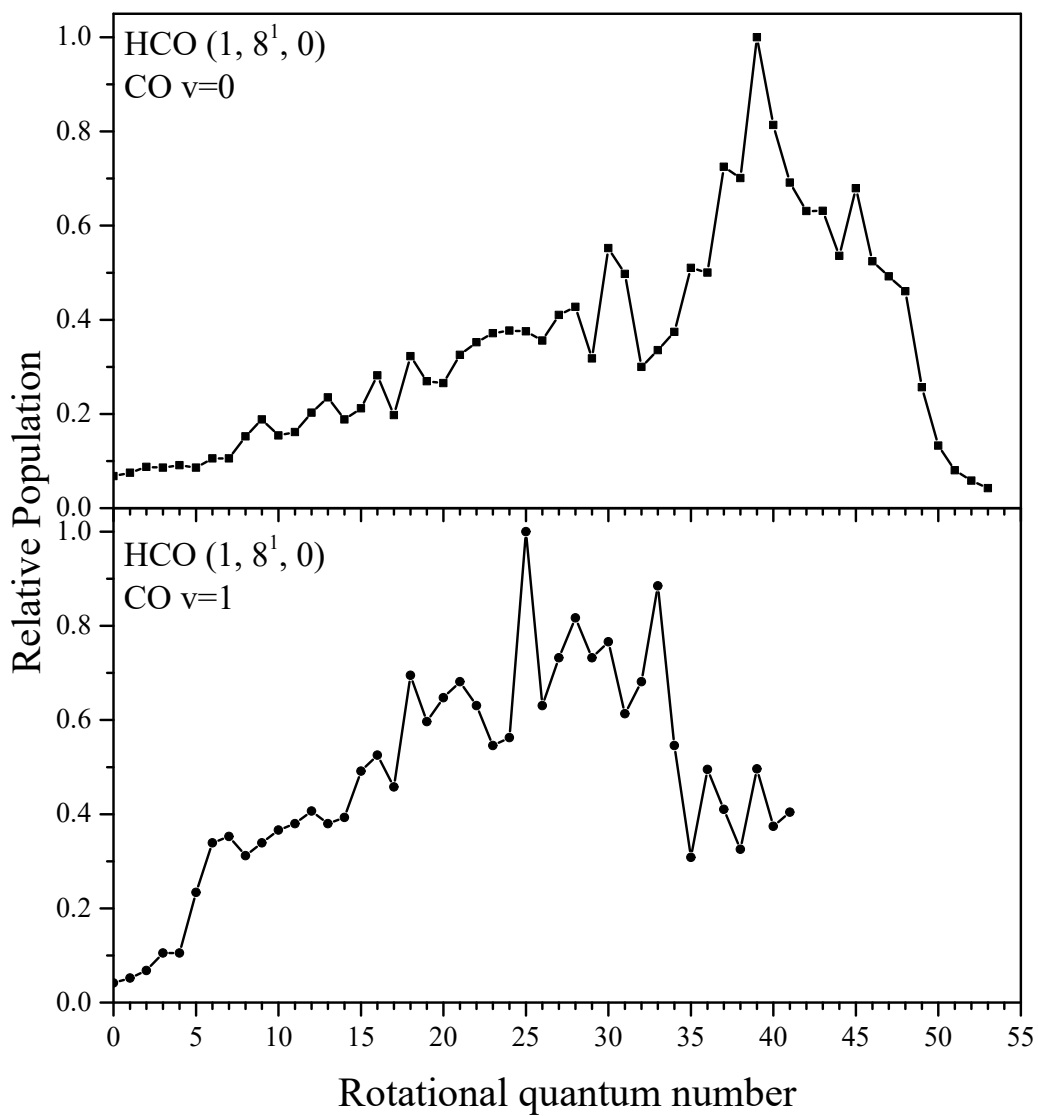


Figure S4. CO ( $X^1\Sigma^+$ ,  $v=0$  and 1) product rotational state distributions from the photodissociation of the HCO  $\tilde{A}^2A''(1, 8^1, 0)$  state.



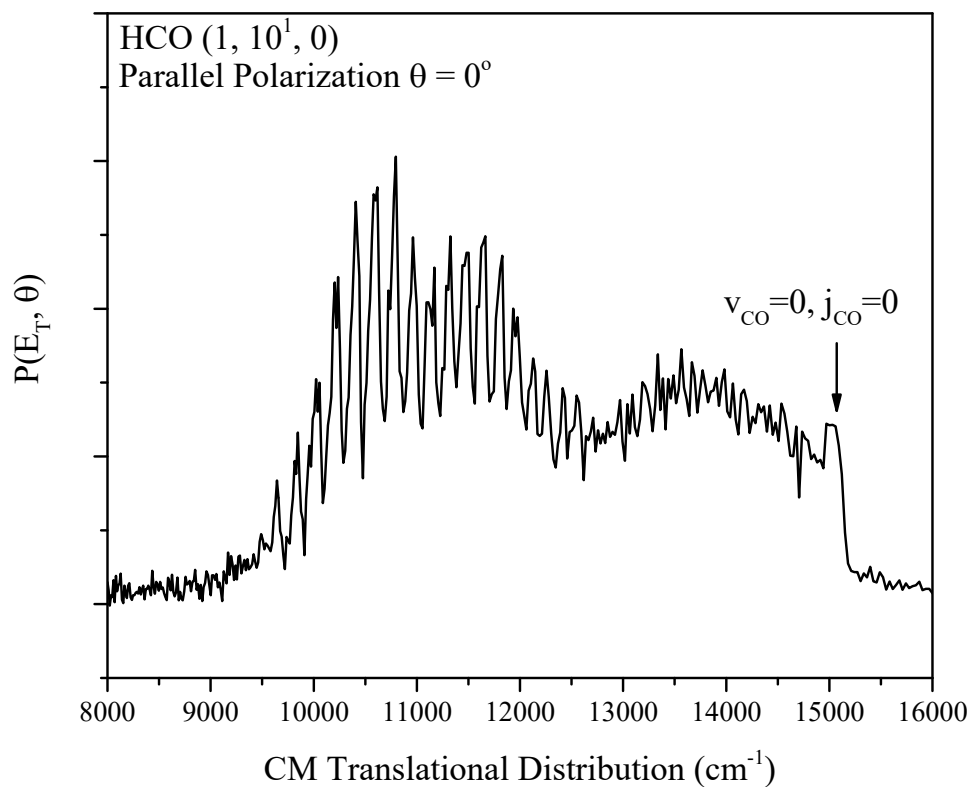


Figure S5. H + CO product CM translational energy distributions from the photodissociation of the HCO  $\tilde{A}^2A''$  (1, 10<sup>1</sup>, 0) state. The product translational energy of the rovibrational ground state ( $v=0, j=0$ ) CO product is indicated by an arrow.

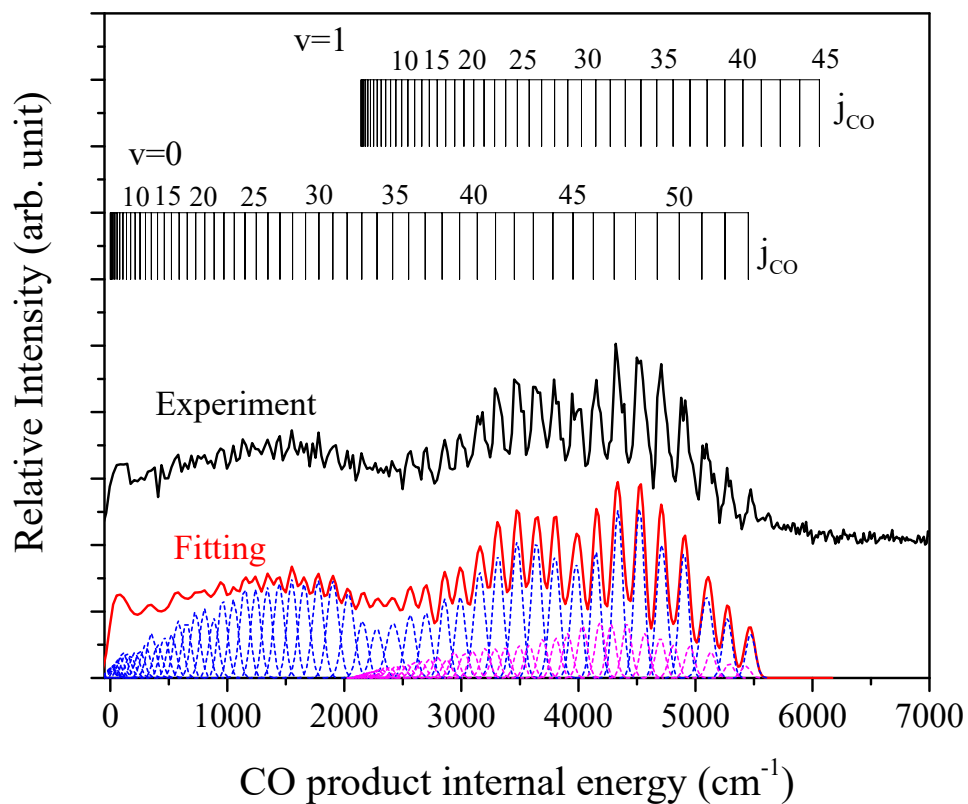


Figure S6. CO ( $X^1\Sigma^+$ ,  $\nu=0$  and 1) product internal energy distribution and the fitting result for the photodissociation of the HCO  $\tilde{A}^2A''(1, 10^1, 0)$  state. The blue and purple dot lines are the Gaussian peaks for each CO product rovibrational state for  $\nu=0$  and  $\nu=1$  levels, respectively. The red solid line is the sum of the Gaussian peaks.

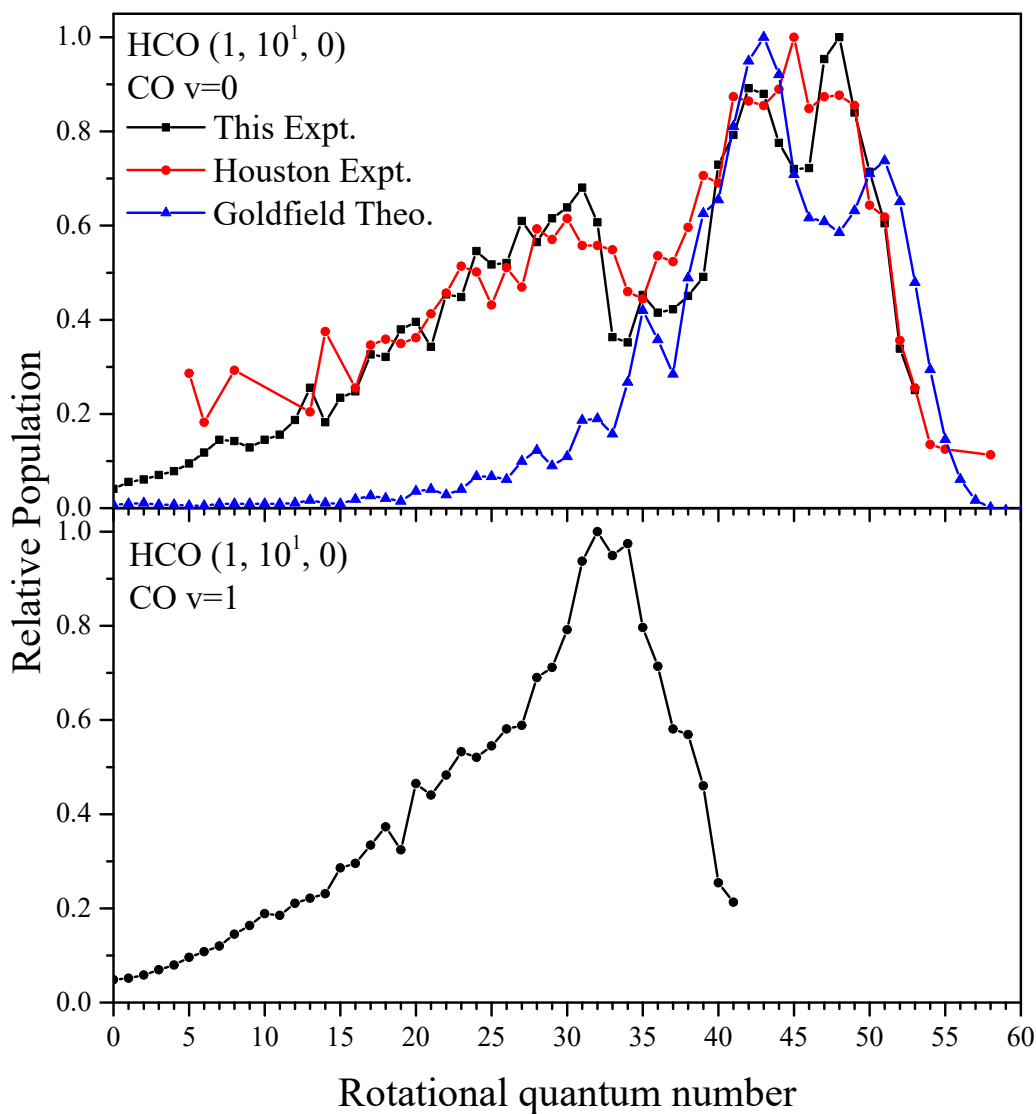


Figure S7. CO ( $X^1\Sigma^+$ ,  $\nu=0$  and 1) product rotational state distributions from the photodissociation of the HCO  $\tilde{A}^2A''(1, 10^1, 0)$  state. The black dots are the data from this experiment, the red dots are experimental data from Houston and coworkers (Figure 7 from Ref. 2), and the blue dots are theoretical data from Goldfield and coworkers.<sup>1</sup>

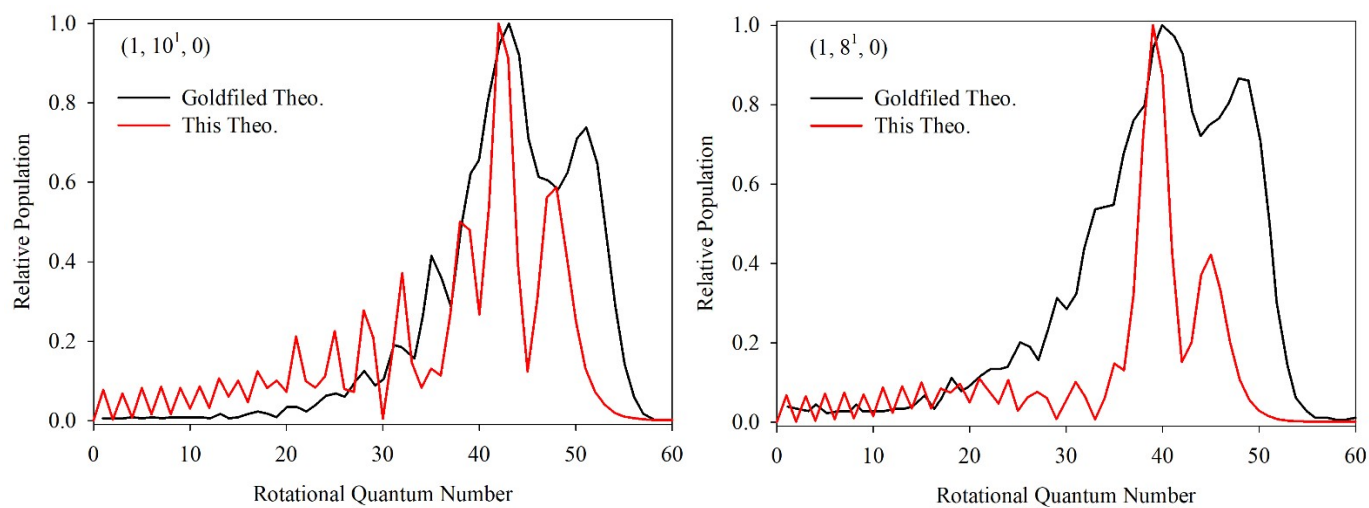


Figure S8. The calculated rotational distribution of  $(1, 10^1, 0)$  and  $(1, 8^1, 0)$  at the transition  $J = 1 \leftarrow J_i = 0$ , compared with the result of Goldfield and coworkers.<sup>1</sup>

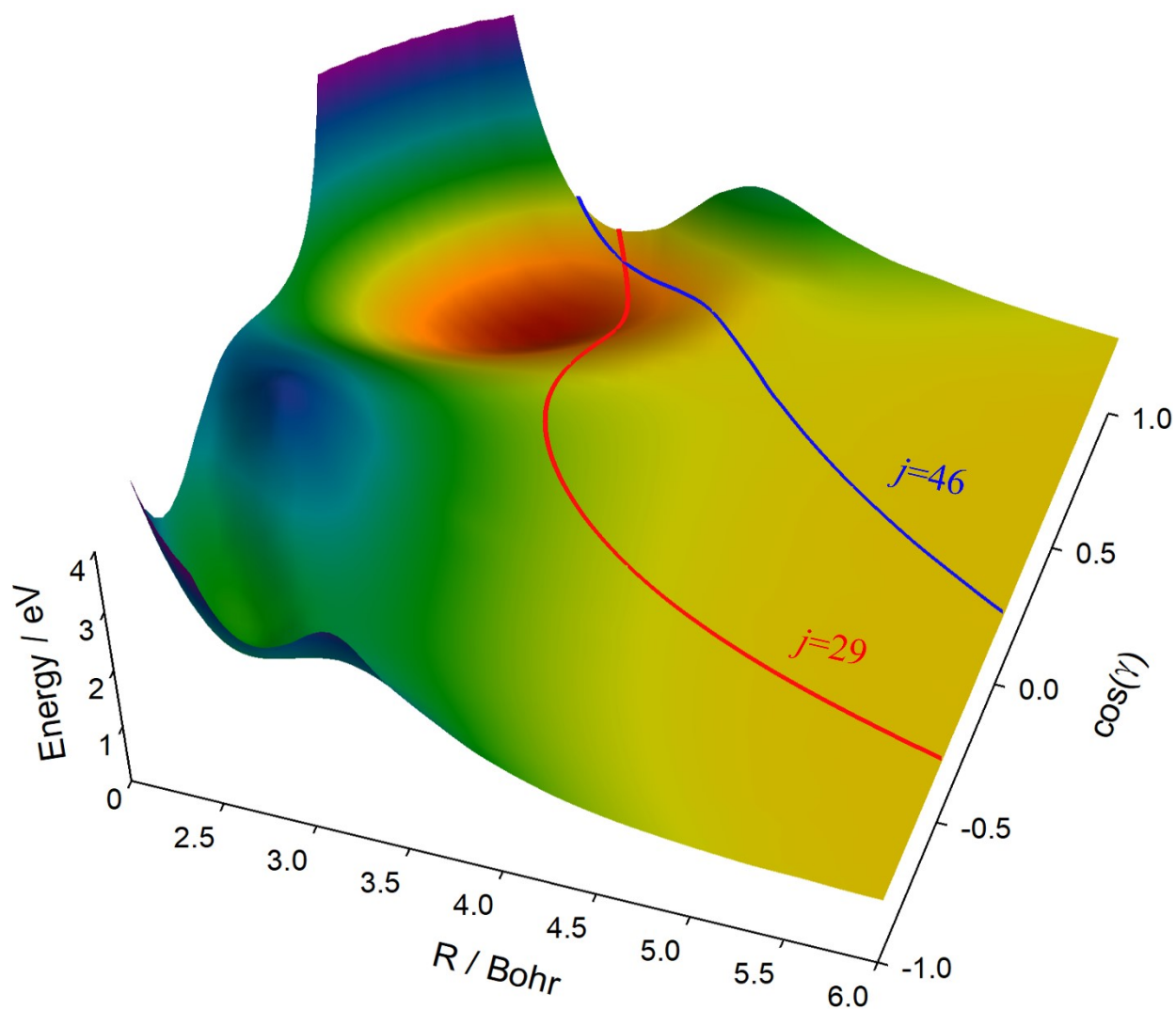


Figure S9. Surface plot of the  $\tilde{X}^c$  state. The CO bond is fixed 2.28 Bohr. The red line and blue line are two typical two-dimensional trajectory simulating  $(0, 10^1, 0)$  and  $(1, 10^1, 0)$ , respectively. The two-dimensional model is referred to our previous study<sup>3</sup>, in which the CO bond is also fixed 2.284 Bohr. The former trajectory starts at the equilibrium ( $R=3.32$  Bohr), while the latter starts at the inner turning point ( $R=3.08$  Bohr).  $j$  denotes the classical rotational angular momentum.